Experimental investigation of the air–fuel charging process in a four-valve supercharged two-stroke cycle GDI engine

Macklini Dalla · Thompson Diórdinis Metzka Lanzanova[1] · Mario Eduardo Santos Martins[1] · Paulo Romeu Moreira Machado[1] · Hua Zhao[2]

Abstract

Fuel consumption standards imposed in several countries for the next years have prompted the development of hybrid passenger cars with ever smaller internal combustion engines. In such powertrain, fuel consumption is as important as engine packaging and power density, so two-stroke engines may be an option due to their higher combustion frequency compared to four-stroke engines. Therefore, the present research investigates the air–fuel charging process of an overhead four-valve direct injection supercharged engine operating in the two-stroke cycle. The optimum start of fuel injection was evaluated for commercial gasoline by means of indicated and combustion efficiencies where a trade-off was found between early and late fuel injections. By advancing the injection timing, more fuel was prone to short circuit to the exhaust during the valve overlap, while late injections resulted in poor charge preparation. The gas exchange parameters, i.e. charging and trapping efficiencies, were obtained from seventy operating points running at fuel-rich conditions. The Benson–Brandham mixing-displacement scavenging model was then fit to the experimental data with a coefficient of determination better than 0.95. With such model, the air trapping and charging efficiencies could be estimated solely based on the scavenge ratio and exhaust lambda, regardless of the engine load, speed, or air/fuel ratio employed. Further twenty-five different lean-burn testing points were tested to certify the proposed methodology applied to the poppet valve two-stroke engine. The in-cylinder lambda was calculated and found different from the exhaust lambda due to mixing between burned gases and intake air during the scavenging process.

Keywords Two-stroke cycle engine · Overhead poppet valves · Fuel injection timing · Gasoline direct injection · Benson–Brandham scavenging model · Lean-burn combustion

Abbreviations

ATDC	After top dead centre
CA	Crank angle
CE	Charging efficiency
DI	Direct injection
EGR	Exhaust gas recycling
EVC	Exhaust valve closing
EVO	Exhaust valve opening
GDI	Gasoline direct injection
IMEP	Indicated mean effective pressure
IVC	Intake valve closing
IVO	Intake valve opening
K	Water–gas equilibrium constant
LHV_{fuel}, LHV	Lower heating value of fuel
LHV_{H_2}	Lower heating value of hydrogen
LHV_{C}	Lower heating value of solid carbon
LHV_{CO}	Lower heating value of carbon monoxide
LHV_{UHC}	Lower heating value of unburned hydrocarbons
m_{air}	Intake air mass per cycle
$m_{trap\ air}$	In-cylinder trapped air mass per cycle
$\dot{m}_{air}$	Air mass flow rate
$\dot{m}_{fuel}$	Fuel mass flow rate
$\dot{m}_{soot}$	Mass flow rate of soot
$\dot{m}_{CO}$	Mass flow rate of carbon monoxide
$\dot{m}_{H_2}$	Mass flow rate of hydrogen
$\dot{m}_{UHC}$	Mass flow rate of unburned hydrocarbons

[1] Engines Research Group (GPMOT), Federal University of Santa Maria, Roraima Av., no 1000, Santa Maria, RS 97105-900, Brazil

[2] Centre for Advanced Powertrain and Fuels Research (CAPF), Brunel University London, Kingston Lane, Uxbridge, Middlesex UB8 3PH, UK

NOx	Oxides of nitrogen
PFI	Port fuel injection
rpm	Revolutions per minute
R^2	Coefficient of determination
SC_{air}	Air short-circuiting
SI	Spark ignition
SOI	Start of fuel injection
SR	Scavenge ratio
SR_{pd}	Scavenge ratio of perfect displacement
TE_{air}	Air trapping efficiency
TE_{fuel}	Fuel trapping efficiency
TWC	Three-way catalyst
UHC	Unburned hydrocarbons
V_{clr}	Clearance volume
V_{ivc}	In-cylinder volume at intake valve closure
y	Hydrogen-to-carbon ratio
[CO]	Volumetric exhaust carbon monoxide concentration
[NOx]	Volumetric exhaust nitrogen oxides concentration
[soot]	Soot concentration
[UHC]	Volumetric exhaust unburned hydrocarbons concentration
η_c	Combustion efficiency
λ	Relative air/fuel ratio (lambda)
λ_{cyl}	In-cylinder lambda
λ_{exh}	Exhaust lambda
ρ_{int}	Intake air density

1 Introduction

The global liquid fuel demand for combustion in the transport sector is currently estimated at about 50 million oil-equivalent barrels per day [1]. Based on this scenario and following the expected world economic growth, the fuel demand for transportation will more than double by 2040 if fuel savings (through more efficient vehicles) are not to be implemented. According to the EU Parliament, by 2020 the EU average passenger car should have a fuel consumption of 3.8 l/100 km, or 95 gCO_2/km, with gasoline [2]. Such limit may be hard to achieve even with over-expanded downsized engines [3], so powertrain hybridisation and lean combustion concepts are possible options.

Lean-burn combustion, either through conventional direct injection [4] or pre-chambers [5], has the potential to improve fuel consumption in spark ignition (SI) engines over conventional homogeneous stoichiometric charging [6]. The gains in fuel consumption resulted from lower pumping losses and higher ratio of specific heats are claimed in the range from 20 to 30% [7, 8]. However, the excess of air available during this combustion process inhibits the effective reduction of NOx emissions by currently employed three-way catalysts (TWC). Methods to reduce NOx emissions with lean-burn combustion are largely used in diesel aftertreatment, although these systems are still commercially prohibitive for small SI engine applications.

While battery electric vehicles (BEV) still face a trade-off between energy storage cost and vehicle range, in plug-in hybrid electric vehicles (PHEV) the limitation of battery energy density (1.2 MJ/dm^3 [9] vs. 32 MJ/dm^3 of gasoline) is mended by the adoption of a combustion engine to improve vehicle autonomy [10]. In such particular powertrain architecture, the two-stroke cycle engine has been quoted candidate due to its higher power density, reduced weight and compactness compared to four-stroke engines [11–13]. In a comparison between two/four-stroke GDI engines for a 30 kW range extender, both engines demonstrated similar BSFC, though the two-stroke unit was found 15% lighter and 38% more compact [14]. The power generation with two-stroke engines may also take advantage of the more frequent firing operation to linearly arrange the cylinder as a free-piston engine [15–17]. Mechanical simplicity, elimination of side forces and variable compression ratio are among the advantages of such concept [18, 19].

Despite the advantages of the two-stroke cycle, conventional crankcase scavenged two-stroke engines often present drawbacks such as excessive unburned hydrocarbon (UHC) emissions [20], crank train lubrication complexity [21] and combustion stability issues [22]. Such disadvantages may be enhanced by the adoption of the four-stroke engine architecture with a wet sump, overhead valves and direct injection, in the so called two-stroke poppet valve engine [23–25]. In this concept, the scavenging of burned gases is performed through conventional overhead valves at a positive intake–exhaust pressure ratio during a long valve overlap (usually more than 120° CA). Even though fuel short-circuiting is reduced by proper timing in DI engines, the exhaust gas dilution by intake air reduces its temperature and still hinders NOx conversion in conventional TWC. In this sense, conventional diesel combustion [26] and low-temperature combustion have been also evaluated [27, 28].

To reduce the dependency on computational fluid dynamics (CFD) simulation and/or test rigs to evaluate the gas exchange parameters of two-stroke engines, e.g. air trapping and charging efficiency, several scavenging models have been developed [29, 30]. Among the multi-zone and multi-phase scavenging models, the one proposed by Benson–Brandham [31] has been successfully applied to loop, cross and uniflow scavenged two-stroke engines. Although the scavenging process is strongly dependent on the engine geometry, this model allows the tuning of two semiempirical parameters. The mixing-displacement two-zone two-phase model of Benson–Brandham assumes that the scavenging process occurs at uniform in-cylinder pressure and volume with no heat transfer across the zones. The term "zones"

refers to the in-cylinder regions containing fresh charge, combustion products, and a mixture of both. Meanwhile, the term "phases" denotes the sequence of events in time, i.e. displacement, mixing, and short-circuiting [32].

In this context, the present research investigates the gas exchange process and the effects of gasoline injection timing in a two-stroke cycle engine embedded in the architecture of a contemporary four-stroke supercharged engine. A multi-zone multi-phase scavenging model developed for conventional ported two-stroke engines is for the first time applied to a poppet valve engine. Hence, charging and trapping efficiency, as well as the in-cylinder lambda, can be determined at any engine operating condition after the model calibration at fuel-rich conditions.

2 Experiments

2.1 Experimental setup

The experiments were performed in Ricardo Hydra single-cylinder engine equipped with an electrohydraulic fully variable valve train unit (Table 1). The side-mounted fuel injector was positioned in such way that the spray pattern was majorly horizontal, so that fuel impingement on the piston top could be minimised at late start of fuel injections as required in the two-stroke cycle (Fig. 1). It could also take advantage of the engine's large bore-to-stroke ratio (1.22) to reduce fuel impingement on the liner as well. Constant speed tests at ± 5 rpm were performed on a transient dynamometer. Engine oil and coolant temperatures were kept at 353 ± 3 K. The fuel used, European gasoline RON 95, was maintained at a temperature and pressure of 293 ± 5 K and 15.0 ± 0.5 MPa, respectively. Fuel and air mass flow rates were measured by an Endress+Hauser Coriolis Promass 83A (maximum error of ± 0.2%) and a Hasting HFM-200 laminar flow meter (maximum error of 1%), respectively. The boosted intake air necessary for the two-stroke operation was supplied by an AVL 515 compressor unit at 300 ± 5 K. Intake and exhaust pressures were measured by two Kistler piezo-resistive transducers, with a maximum error of ± 0.1% each. The average flow temperatures were measured by

Table 1 Engine specifications

Engine model	Ricardo Hydra Camless Two/four-stroke
Displaced volume	0.35 dm^3
Bore × stroke	81.6 × 66.9 mm
Compression ratio	11.8:1
Combustion chamber	Four valves pent-roof with central sparkplug
Fuel	UK commercial gasoline RON 95
Fuel injector	Solenoid type Magneti Marelli IHP 072 asymmetrical six holes
Exhaust valve opening (EVO)	120° CA ATDC
Intake valve opening (IVO)	130° CA ATDC
Exhaust valve closing (EVC)	230° CA ATDC
Intake valve closing (IVC)	240° CA ATDC
Valve lift	8.0 mm

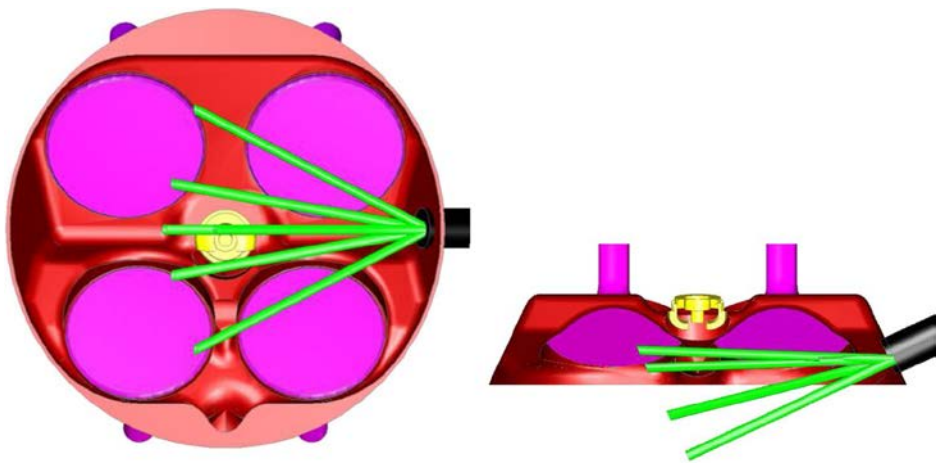

Fig. 1 Combustion chamber geometry and fuel injector position with approximate spray pattern [33]. The second image is a cross section of the chamber at the sparkplug plane, with the intake valves (smaller) at the back

K-type thermocouples with ± 1% accuracy. An AVL GH15D piezo-electric transducer was used to measure the in-cylinder pressure with maximum error of ± 0.3%. It was correlated to the crankshaft position through a LeineLinde incremental encoder with 720 pulses per revolution. Emissions of unburned hydrocarbons (UHC), carbon monoxide (CO), carbon dioxide (CO_2), oxygen (O_2), and oxides of nitrogen (NOx) were analysed by a Horiba MEXA 7170DEGR with an error smaller than 2%. Smoke values were measured with an AVL 415 with a repeatability better than 3%. A NI 6353 USB X card was employed for data acquisition purposes. All test results were averaged over 200 consecutive engine cycles.

To improve the scavenging process through a reverse tumble, as well as reduce the air short-circuiting to the exhaust during the valve overlap, a 3-mm-high mask was mounted on the cylinder head as shown in Fig. 2. The spark timing was either set to minimum advance for best torque (MBT) or knock limited advance, depending upon the engine load and speed. The engine's cyclic variability was evaluated by the coefficient of variation of IMEP (COV_{IMEP}), and it was limited to 10% considering its more frequent combustion compared to four-stroke engines [34]. The pressure rise rate was used to identify abrupt combustion, and a limiting value of 0.5 MPa/°CA was chosen based on other studies with similar engine specifications [35, 36]. More details of the experimental setup, including a schematic representation of the research engine and test cell facilities, can be found elsewhere [37].

2.2 Overall test procedure

The engine was firstly tested with fuel-rich early SOI timings (next to EVC) to provide enough data for the Benson–Brandham scavenging model calibration. In total, seventy operating points were tested at various engine loads and speeds in the range 0.2–1.0 MPa IMEP and 800–2400 rpm, respectively. Next in time, the SOI optimisation process at lean-burn conditions was set up and a sweep of at least eight different injection timings was carried out 40° CA around IVC to find the trade-off between early and late SOIs. At this stage, the engine load was varied from 0.2 to 1.0 MPa IMEP with increments of 0.2 MPa, while the engine speed was evaluated every 400 rpm from 800 to 2400 rpm. As a result, 25 optimum SOI timings (based on indicated efficiency) were obtained. Finally, by means of the properly calibrated Benson–Brandham scavenging model, gas exchange parameters, i.e. charging and air trapping efficiency, as well as the in-cylinder lambda, could be estimated at those 25 optimised operating points.

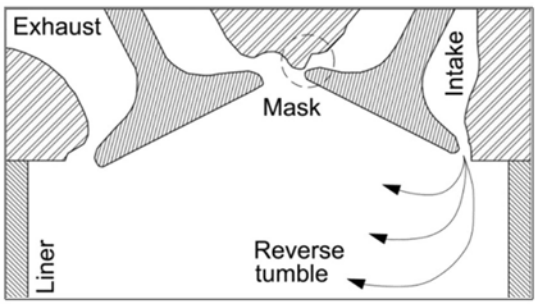

Fig. 2 Cross section of the combustion chamber at the valve plane [38]

2.3 Determination of optimum start of injection (SOI) timings

Indicated and combustion efficiencies were used to evaluate the compromise between early and late fuel injections. Engine loads from 0.2 to 1.0 MPa IMEP were tested with increments of 0.2 MPa, while the engine speed was varied from 800 to 2400 rpm in steps of 400 rpm.

The combustion efficiency was calculated based on the combustible species (CO, UHC, H_2 and soot) found in the exhaust emissions as presented in the following equation [34]:

$$\eta_c = 1 - \frac{\dot{m}_{CO}\mathrm{LHV}_{CO} + \dot{m}_{UHC}\mathrm{LHV}_{UHC} + \dot{m}_{soot}\mathrm{LHV}_{C} + \dot{m}_{H_2}\mathrm{LHV}_{H_2}}{\dot{m}_{fuel}\ \mathrm{LHV}_{fuel}} \quad (1)$$

The LHV values used for CO, UHC, H_2 and soot were 10.1 MJ/kg, 42.5 MJ/kg, 120 MJ/kg and 32.8 MJ/kg (solid carbon), respectively. Hydrogen emissions were estimated based on the Brettschneider–Spindt algorithm [39].

2.4 Procedures for the gas exchange analysis and in-cylinder lambda estimation

In two-stroke engines, the scavenge ratio (SR) is defined as the ratio between the intake air mass supplied per cycle (m_{air}) and the in-cylinder reference mass at intake conditions. The reference volume used to calculate the reference mass was the sum of the clearance volume (V_{clr}) and the in-cylinder volume at IVC (V_{ivc}), at an intake air density p_{int}

$$\mathrm{SR} = \frac{m_{air}}{(V_{ivc} + V_{clr})\ p_{int}} \quad (2)$$

The air trapping efficiency (TE_{air}) relates the in-cylinder trapped air mass ($m_{trap\ air}$) at IVC to the intake air mass supplied per cycle. Several methods have been proposed to measure it under engine firing conditions, such as the exhaust gas sampling valve [40], the tracer gas method [41, 42], and the analysis of exhaust emissions under fuel-rich operation [43]. The last technique is based on the presumption that

any remaining oxygen in the exhaust derives from scavenging inefficiencies, such as mixing scavenging and air short-circuiting. Because of its simplicity, this method was chosen as presented in the following equation [44]:

$$TE_{air} = \frac{m_{trap\ air}}{m_{air}} = \frac{0.5[CO] + \left(1 - \frac{yK}{[CO]+K[CO_2]}\right)[CO] + 0.5[NOx]}{0.5[CO] + [CO_2] + [O_2] + 0.25\frac{yK}{[CO]+K[CO_2]}[CO] + 0.5[NOx]} \quad (3)$$

The terms between brackets represent the volumetric concentrations of each gas in the exhaust, while y is the hydrogen-to-carbon ratio of the fuel and K is the water–gas equilibrium constant (considered to be equal to 3.5).

The charging efficiency was calculated by the ratio between the in-cylinder trapped air mass at IVC and the in-cylinder reference mass at intake conditions. By definition, it results from the product between scavenge ratio and air trapping efficiency as seen in the following equation:

$$CE = \left(\frac{m_{trap\ air}}{V_{ivc} + V_{clr}}\right)\Big/ p_{int} = SR * TE_{air} \quad (4)$$

Under idealised flow conditions, the in-cylinder charge and burned gases may assume identical densities [43], so the internal EGR fraction can be inferred from the difference between the charging efficiency and the unit, e.g. a charging efficiency of 0.65 represents approximately a residual gas (or internal EGR) fraction of 0.35.

Due to scavenging inefficiencies, such as mixing between intake air and burned gases and air short-circuiting to the exhaust, the measured overall relative air/fuel ratio (lambda) differed from the in-cylinder lambda. The in-cylinder lambda (λ_{cyl}) was then calculated based on air and fuel trapping efficiencies, TE_{air} and TE_{fuel}, respectively.

$$k_{cyl} = k_{exh}\left(\frac{TE_{air}}{TE_{fuel}}\right) \quad (5)$$

The overall exhaust lambda (λ_{exh}) was calculated based on gaseous emissions according to the algorithm developed by Brettschneider–Spindt [39], which yields more accurate results than conventional UEGO sensors. The fuel trapping efficiency was calculated based on the exhaust emissions of CO, CO_2, and UHC, as presented in the following equation [44]:

$$TE_{fuel} = \frac{[CO] + [CO_2]}{[CO] + [CO_2] + [UHC]} \quad (6)$$

The inclusion of the TE_{fuel} in the calculation of the in-cylinder lambda aimed at considering any short-circuited fuel; if not measured, it would under-predict the real in-cylinder lambda. The adoption of direct fuel injection was able to remove the fuel short-circuiting issue from two-stroke engines, although the short time available for air–fuel mixing often results in unburned fuel at EVO.

In order to obtain higher thermal and combustion efficiencies, lean-burn combustion should be employed instead of fuel-rich charging (used to assess the in-cylinder lambda). Hence, it is proposed to run the two-stroke poppet valve engine at fuel-rich conditions and early injections to form a homogeneous mixture, so that the gas exchange data obtained can be employed to calibrate the Benson–Brandham scavenging model [31]. According to this theory, the scavenging is firstly subjected to a displacement process until it reaches a certain value of scavenge ratio. After this point, the fresh air and the burnt gases are more prone to mix up to the end of the scavenging process. The $TE_{air} \times SR$ and $CE \times SR$ curves obtained are essentially constant independent of the fuel, engine load or speed tested, as long as the valve parameters and engine geometric features are not changed. Once determined the constants of the scavenging model, any value of scavenge ratio (easily measured from an experimental point of view as seen in Eq. 2) could be translated into values of charging and trapping efficiency even at lean-burning conditions.

To apply the Benson–Brandham scavenging model to the poppet valve engine, its cylinder was divided into two zones: a mixing zone near the intake valves and a burned gas zone close to the exhaust valves. The fresh charge was considered mixed with the burned gases adjacent to the intake valves, while close to the exhaust valves the burned gas zone remained unaffected while leaving the cylinder. By the time that all the burned gas contained in the region close to the exhaust valves had left the cylinder, the second phase of the Benson–Brandham model started and only mixing scavenging occurred. Apart from the two zones mentioned (mixing and burned gas zones), a third zone, the air short-circuiting zone, was considered throughout the phases. In the original work of Benson and Brandham, the short-circuiting term was not considered, although later research added this parameter [29, 43]. Figure 3 shows a schematic view of this extended Benson–Brandham model applied to the engine geometry.

The end of the first phase of the scavenging process, called perfect displacement, occurred at an engine-dependent value of scavenge ratio (SR) known as the

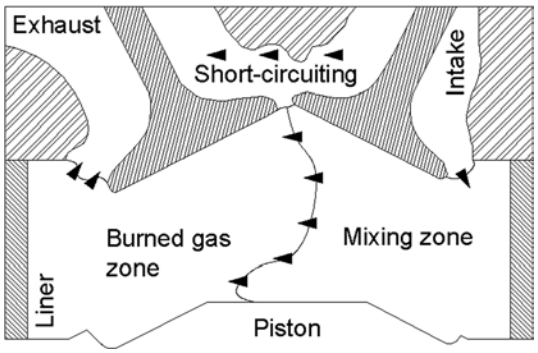

Fig. 3 Representation of the extended Benson–Brandham scavenging model applied to the two-stroke poppet valve engine

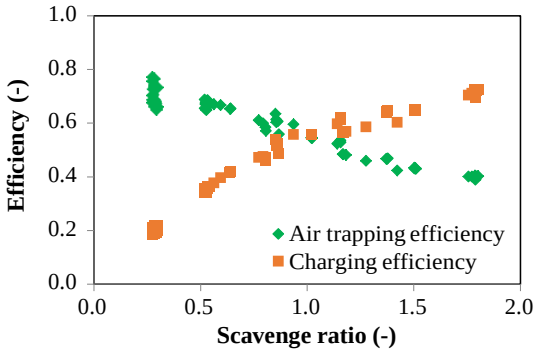

Fig. 4 Air trapping and charging efficiencies as a function of scavenge ratio

scavenge ratio of perfect displacement (SR_{pd}). After this, the scavenging process was conducted under perfect mixing between the incoming charge and the burned gases. Hence, there were two equations used to calculate the air trapping efficiency:When:

$$SR \leq \left(\frac{SR_{pd}}{1 - SC_{air}}\right) \tag{7}$$

Then:

$$TE_{air} = 1 - SC_{air}. \tag{8}$$

And when:

$$SR > \left(\frac{SR_{pd}}{1 - SC_{air}}\right) \tag{9}$$

Then:

$$TE_{air} = \frac{1 - \left(1 - SR_{pd}\right) / e^{(SR_{pd} - (1 - SC_{air})SR)}}{SR} \tag{10}$$

Equation 8 was used for SR values less than or equal to the SR_{pd}, while Eq. 10 was employed for SR values greater than the SR_{pd}. The air short-circuiting term (SC_{air}) was included as a reducer of the scavenge ratio and hence shifted up the critical scavenge ratio.

3 Results and discussion

3.1 Benson–Brandham scavenging model calibration

The engine was tested at several speeds and loads at fuel-rich conditions, so that the gas exchange parameters presented in Sect. 2.4 could be estimated. In Fig. 4, it is presented the operating points with air trapping efficiency and charging efficiency as a function of the scavenge ratio. As the scavenge ratio increased, the charging efficiency improved due to the larger fraction of air delivered on a time basis. However, the air trapping efficiency dropped as more air was mixed with the burned gases and short-circuited to the exhaust. It can be seen that the air trapping and charging efficiencies were solely dependent on the scavenge ratio irrespective of the engine speed or load. At a constant intake pressure, the higher the engine speed the shorter was the time available for the gas exchange on a time basis and hence the lower was the scavenge ratio. On the other hand, at higher engine loads (higher intake pressures) the scavenge ratio and charging efficiency increased at the expense of air trapping efficiency.

From the experimental data presented in Fig. 4, it was possible to correlate scavenge ratio and air trapping efficiency with the extended Benson–Brandham model. As there were no direct measurements of the scavenge ratio of perfect displacement and air short-circuiting terms, an iterative process was used to fit the experimental data through Eqs. 8 and 10. The coefficient of determination (R^2) was used to indicate the most appropriate values of SR_{pd} and SC_{air}, resulting in the lowest residual between the extended Benson–Brandham curve and the data points. The most suitable trend line is presented in Fig. 5 alongside the experimental results and the perfect mixing model from Hopkins [30] for comparison purposes.

From Fig. 5, it is possible to identify the transition from displacement scavenging to mixing scavenging, given by the inflexion in the Benson–Brandham curve at 0.49 of scavenge ratio. The correlation between this scavenging model and the data acquired was considered satisfactory with a R^2 close to 0.946 for the seventy testing points obtained with early SOI and fuel-rich mixtures. Through successive iterations, the optimum values for SR_{pd} and SC_{air} to be used in Eqs. 8 and 10 were found to be 0.342 and 0.300, respectively. Therefore, the air trapping efficiency became a function of the scavenge ratio only (Eq. 2). Compared to the perfect mixing model from Hopkins, the two-stroke poppet valve engine

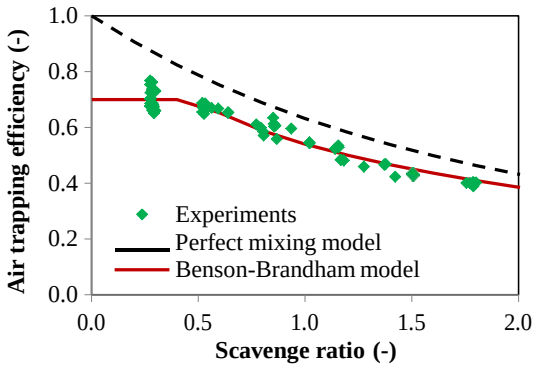

Fig. 5 Application of the Benson–Brandham scavenging model to the experimental results. Perfect mixing model [30] displayed for comparison purposes

performance was considered poor, as the majority of ported engines yield results above such curve [43]. This includes the recent development in uniflow two-stroke opposed-piston diesel engines [45, 46].

Alongside the scavenge ratio, the fuel trapping efficiency (TE_{fuel}) and the exhaust lambda were the two remaining parameters necessary to estimate the in-cylinder lambda regardless of the engine operating conditions. By using direct fuel injection, only air was employed to scavenge the burned gases and hence higher values of TE_{fuel} were expected in comparison with mixture scavenged two-stroke engines. However, it is sometimes convenient to advance the SOI to improve the mixture formation, but at the expense of poorer fuel trapping efficiency. Figure 6 presents the in-cylinder lambda prediction based on scavenge ratio at fuel trapping efficiencies of 0.9 (left) and 1.0 (right).

Figure 6 shows the linear correlation between exhaust lambda and in-cylinder lambda until the critical scavenge ratio of 0.49. At this point, the mixing phase of the scavenge process begun and the air trapping efficiency started dropping from its constant value. A constant air short-circuiting value of 0.3 was considered in the determination of the critical SR in Eqs. 7 and 9. After this transition, the exhaust lambda increased linearly with the scavenge ratio, though the curves were proportionally shifted downwards as the fuel trapping efficiency decreased from 1.0 to 0.9. All curves diverged as the scavenge ratio and exhaust lambda increased, due to the exponential behaviour of Eq. 10. The relationship between scavenge ratio, exhaust lambda, fuel trapping efficiency, and in-cylinder lambda presented in Fig. 6 can be analytically expressed as:When:

$$SR \leq 0.49, \tag{10}$$

Then:

$$k_{cyl} = k_{exh}\left(\frac{0.7}{TE_{fuel}}\right). \tag{11}$$

And when:

$$SR > 0.49, \tag{12}$$

Then:

$$k_{cyl} = k_{exh}\left(\frac{1-0.658e^{(0.342-0.7SR)}}{TE_{fuel}SR}\right) \tag{13}$$

Therefore, for this particular engine operating with a constant valve timing and lift, the in-cylinder lambda could be estimated even at lean-burn conditions. The requirements in this case were the tailpipe exhaust lambda (λ_{exh}), scavenge ratio (SR) given by Eq. 2, and fuel trapping efficiency (TE_{fuel}) given by Eq. 6.

Fig. 6 In-cylinder lambda estimation as a function of exhaust lambda and scavenge ratio at different fuel trapping efficiencies (TE_{fuel} = 0.9 on the left side and TE_{fuel} = 1.0 on the right side)

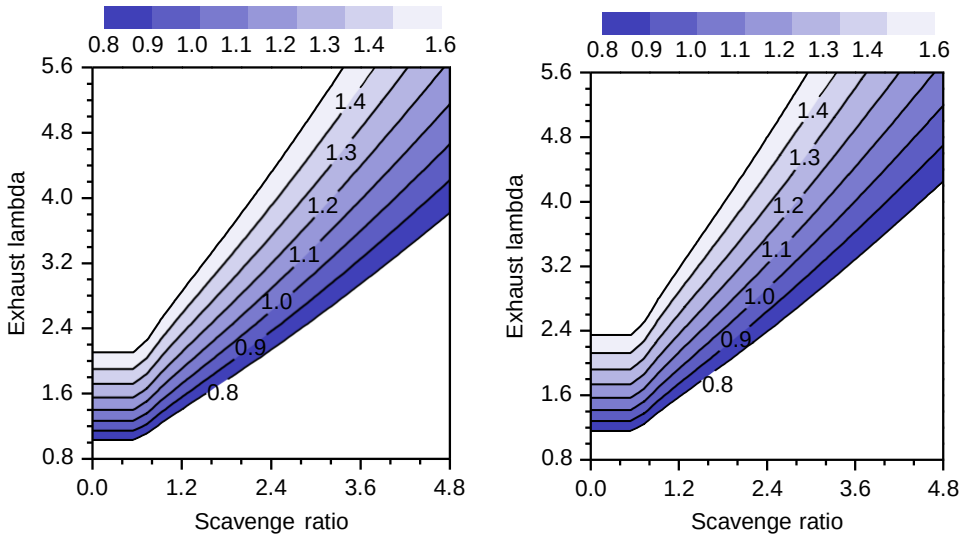

3.2 Determination of optimum start of injection timings

Figure 7 presents the indicated efficiency as a function of the SOI at the limiting speeds and loads evaluated, i.e. 800 rpm and 2400 rpm and 0.2 MPa and 1.0 MPa IMEP. To avoid clustering, only four operating points around the maximum indicated efficiency were presented for each case. In all cases, the indicated efficiency reached a maximum at a specific start of fuel injection, so advancing or retarding the SOI from this best timing severely deteriorated the engine performance. At early injections, the in-cylinder pressure, temperature and gas density were lower, so the fuel spray had greater penetration towards the liner and possibly resulted in impingement. At even earlier injection timings, before IVC and EVC, fuel short-circuiting to the exhaust took place as evidenced by a sheer increase in UHC emissions. On the other hand, later fuel injections long after IVC may have resulted in fuel impingement on the piston surface and formation of over-rich regions due to the short time available for charge homogeneity. High values of CO and soot were detected in such conditions. It could be also observed that the engine speed had the major impact on the optimum SOI timing. Even though the engine load increased by five times among the cases presented, which meant the fuelling rate increased proportionally, the SOI for best indicated efficiency remained nearly constant at around 215° CA at 2400 rpm and 250° CA at 800 rpm.

The indicated efficiency was found to largely follow the combustion efficiency trend shown in Fig. 8. Early fuel injections resulted in fuel short-circuiting, while later injections resulted in poor air–fuel mixing and incomplete combustion. At lower engine speeds, the time available for air–fuel mixing increased and later start of injections could be used, with associated lower spray penetration. However, as the engine speed increased to 2400 rpm the time available for charge preparation dropped and the SOI had to be advanced by about 35° CA. In this case, it could be inferred that any possible fuel impingement given by earlier injections, particularly on the cylinder liner, was offset by the gains in mixture preparation at longer mixing times. The higher wall temperatures at 2400 rpm resulting from the shorter time available for heat transfer may have also contributed to accelerate the vaporisation of any impinged fuel.

The overall SOI timing map is shown in Fig. 9. The requirement of earlier SOI at higher engine speeds and loads can be observed (particularly high load). In the range of loads and speeds tested, the SOI timing remained between 220° and 270° CA ATDC. At the lowest engine speed and load tested of 800 rpm and 0.2 MPa IMEP, respectively, the SOI was found close to 270° CA ATDC, which was much later than EVC (230° CA ATDC) and IVC (240° CA ATDC) timings. This event denies the presumption that best fuel economy should be obtained with a more homogeneous charge. In fact, in this condition the amount of fuel injected was so small that later injections might have helped to form a more combustible mixture in the vicinity of the sparkplug for a more stable combustion. From Fig. 1, this possibility of fuel stratification due to the injector position is clear, although further computational fluid dynamics simulation is necessary to confirm this assumption.

3.3 Determination of gas exchange parameters and in-cylinder lambda under lean-burn conditions

From the calibration of the Benson–Brandham model, the air trapping and charging efficiencies could be estimated at

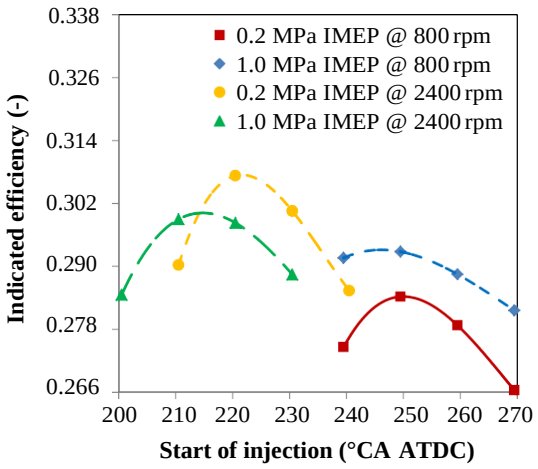

Fig. 7 Indicated efficiency for the SOI sweeps at 800/2400 rpm and 0.2/1.0 MPa IMEP

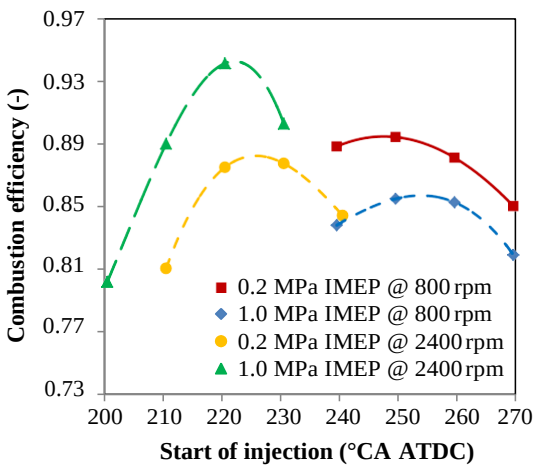

Fig. 8 Combustion efficiency for the SOI sweeps with gasoline at 800/2400 rpm and 0.2/1.0 MPa IMEP

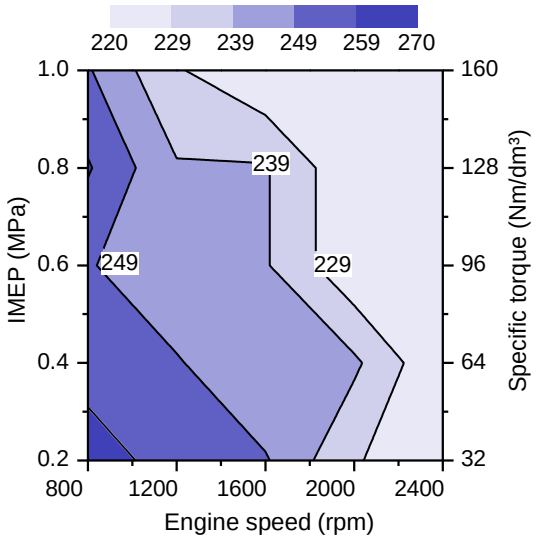

Fig. 9 Injection timing (°CA ATDC) versus engine speed and load

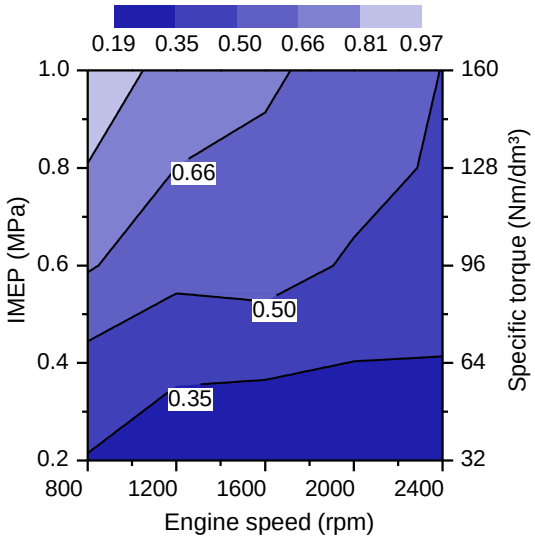

Fig. 10 Charging efficiency (−) versus engine speed and load

lean-burn combustion. Differently from port fuel injection (PFI) engines, or even direct fuel injection (DI) engines with early injections, the fuelling rate had minimum impact on charging efficiency. DI engines have usually higher volumetric efficiencies than PFI engines as the fuel ideally absorbs heat uniquely from the combustion chamber to vaporise, so it does not displace the incoming fresh charge [47]. In the poppet valve two-stroke engine, the SOI took place so close to IVC/EVC that the fuel vaporisation had negligible effect on the induced air mass. As the engine speed increased, the time available for the gas exchange shortened, so the charging efficiency (Fig. 10) reduced and the air trapping efficiency (Fig. 11) increased. At such conditions, the high levels of hot residual gas trapped resulted in abrupt combustion and even controlled auto-ignition as presented elsewhere [38]. Nevertheless, even at higher engine speeds and lower loads the TE_{air} could not exceed 70%, which is a very modest result compared to conventional ported two-stroke engines [20]. Such limiting value resulted from the constant air short-circuiting term (SC_{air}) of 0.3, which also influenced the exhaust gas temperature as previously reported [37].

Figure 12 presents the in-cylinder lambda results obtained through Eqs. 11 and 13 with lean-burn combustion. As the engine load increased at lower speeds, the minimum levels of residual gas trapped and the greater in-cylinder temperatures enabled the achievement of leaner in-cylinder mixtures. Moreover, the higher charge turbulence generated by the larger scavenge ratio (Fig. 13) at such speeds also contributed to increase in the lean-burn limit. The in-cylinder lambda reached 1.34 from 0.5 MPa to 1.0 MPa IMEP below 1100 rpm. At higher engine speeds, the amount of internal EGR raised and the charge heat capacity enlarged, so a richer air/fuel mixture was required to maintain acceptable combustion stability. Values of λ_{cyl} between 1.00 and 1.15 were observed in the largest portion of the operation map, which agrees with the maximum in-cylinder temperature usually observed in four-stroke engines operating at lambda values in the range 1.05–1.10 [48]. Despite the overall lean engine operation, there were regions where richer mixtures were employed. At the extremely diluted combustion at 2400 rpm and 0.2 MPa IMEP, when the internal EGR fraction remained between 0.65–0.81, the in-cylinder lambda was reduced to about 0.90 to improve combustion stability.

The scavenge ratio values seen in Fig. 13 in the operation of the two-stroke poppet valve engine were found above the values usually observed in conventional two-stroke ported

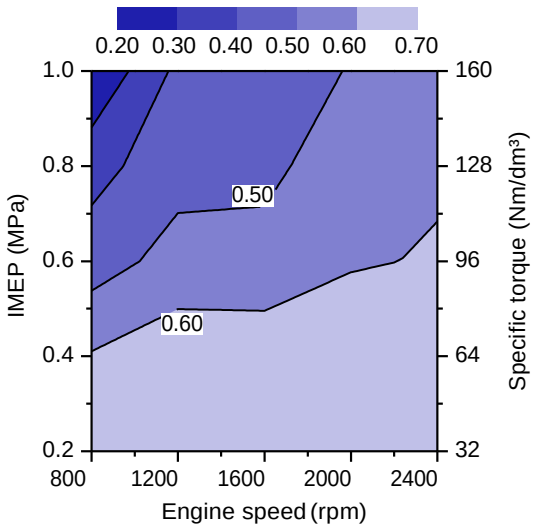

Fig. 11 Air trapping efficiency (−) versus engine speed and load

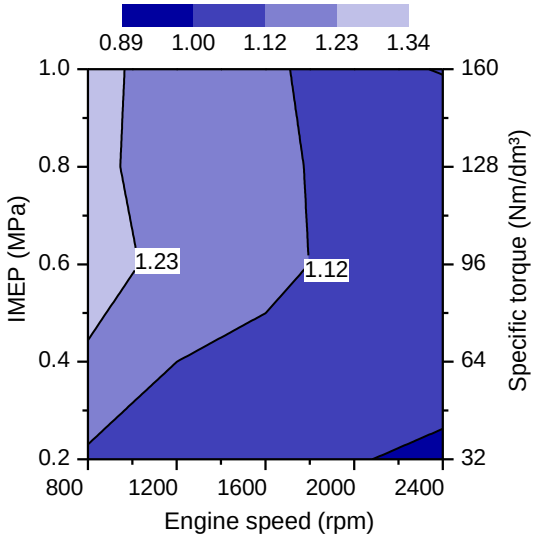

Fig. 12 Approximated in-cylinder lambda (−) versus engine speed and load

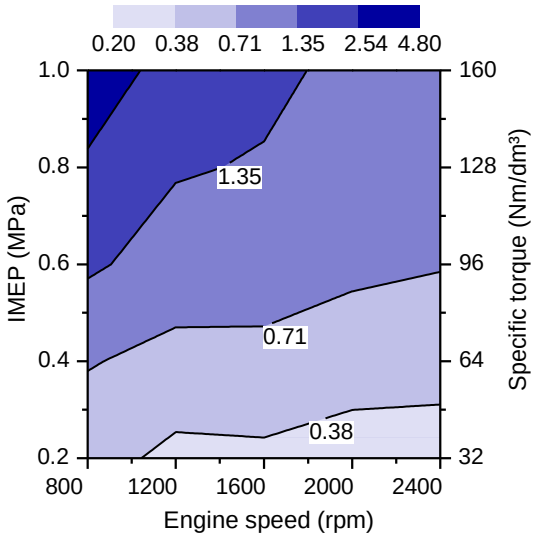

Fig. 13 Scavenge ratio (−) versus engine speed and load

engines [43]. This is mostly attributed to the poor scavenging performance associated with the pent-roof valve arrangement, which allows a large portion of the incoming air to be short-circuited to the exhaust. Also, in crankcase scavenged engines there is a peak intake pressure at the beginning of the scavenge process due to the crankcase compression ratio, which is followed by a reduction in the pressure towards the end of the scavenging. Meanwhile, in externally supercharged engines there is no intake peak pressure so the average pressure (Fig. 14) should be higher during the scavenging for an equivalent engine load.

From Fig. 14, the larger intake pressure requirement at higher engine speeds and loads is clear, while at the lowest load/speed tested a pressure slightly above atmosphere (~105 kPa) is enough for engine operation. Overall, the intake pressure values were found in the range 105–200 kPa, which is commonly achieved in contemporary turbocharged and/or supercharged four-stroke engines. On the other hand, at speeds and loads below 1500 rpm and 0.6 MPa, respectively, the intake pressure remained between 100 and 115 kPa, which is a modest value considering the output torque around 80 Nm/dm^3. A similar four-stroke engine would need to be operated at 1.2 MPa IMEP at the same speed (1500 rpm) to generate a similar output torque, which is often prohibited due to knocking combustion or insufficient boost at such speed [49].

The large scavenge ratio values presented in Fig. 13, particularly at higher loads and lower engine speeds, had a negative impact on the exhaust lambda shown in Fig. 15. The exhaust lambda was found around 1.8 times greater than the in-cylinder lambda. All data points were obtained in the lean-of-stoichiometric region, so conventional TWC could not be used in this case to reduce engine-out emissions, particularly NOx. Also, the higher the exhaust gas dilution by the intake air, the lower was its temperature, which hinders aftertreatment operation and reduces the enthalpy available for possible turbocharging.

The large values of exhaust lambda obtained here, particularly at high loads, could be improved by different valve timings with shorter valve overlap, although this would impact on the maximum load and speed achievable [50]. On the other hand, the redesign of the combustion chamber with a taller mask (Fig. 2) and improved intake port arrangement

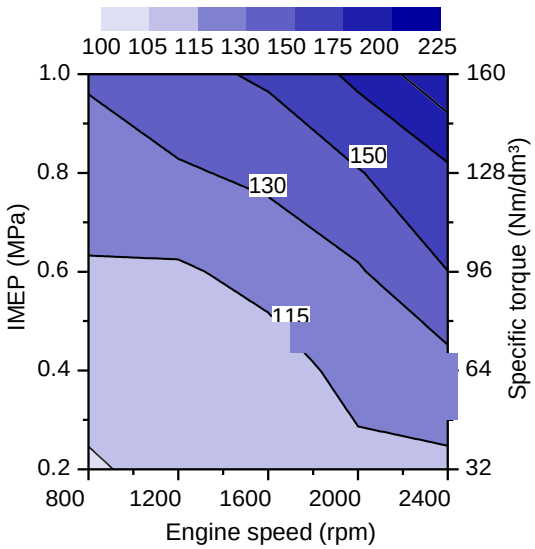

Fig. 14 Intake pressure (kPa) versus engine speed and load

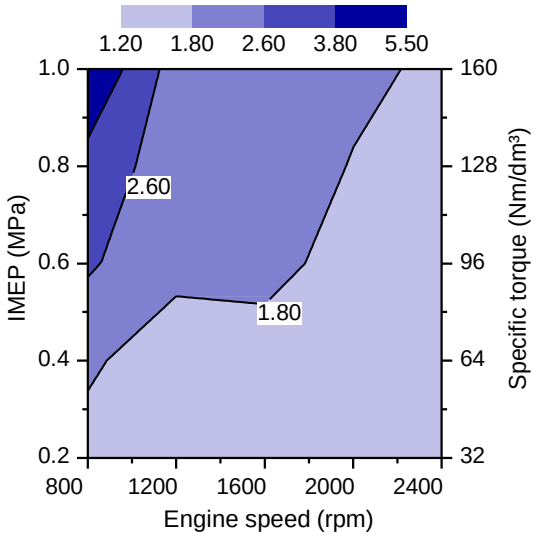

Fig. 15 Tail pipe exhaust lambda (−) versus engine speed and load

[51, 52] could also reduce the exhaust gas dilution, but at the cost of larger air flow restriction.

4 Summary

A four-valve supercharger DI engine was operated in the two-stroke cycle at engine loads and speeds varying in the range 0.2–1.0 MPa IMEP and 800–2400 rpm, respectively. The optimum SOI timing was found through a sweep of 40° CA near IVC until the maximum indicated efficiency could be achieved. The Benson–Brandham scavenging model was successfully applied to the proposed engine so that the gas exchange parameters, i.e. air trapping and charging efficiencies, could be estimated after its calibration at fuel-rich conditions. The in-cylinder lambda was also assessed in this manner, based on scavenge ratio, fuel trapping efficiency, and exhaust lambda.

The optimum SOI was found to follow a very narrow timing window until combustion inefficiencies severely deteriorated the indicated efficiency. The higher the engine speed and load, the more advanced the fuel injection took place to allow a proper charge homogeneity. The effect of engine speed was found more pronounced than that of engine load on the SOI timing.

The higher the engine speed the shorter was the time available for gas exchanging, so the charging efficiency decreased and the air trapping efficiency improved as a smaller amount of air was short-circuited to the exhaust. The air trapping efficiency was found below the values often employed in conventional ported two-stroke engines, particularly above 0.4 MPa IMEP. At load values below this, a roughly continuous air trapping efficiency was obtained as a result of the constant air short circuit term of 0.3 in the Benson–Brandham scavenging model. Such mixing-displacement two-zone two-phase model presented appreciable capacity to express the experimental results and enabled the estimation of air trapping and charging efficiencies even at lean-burn conditions. This methodology is expected to be one more tool to be used in research and development of future two-stroke engines, as well as four-stroke engines with long valve overlap. Nevertheless, one should note that any modification on engine geometry, valve timing or valve lift requires a new curve fitting so the newer scavenge ratio of perfect displacement and air short-circuiting terms can be obtained through iteration.

In several regions, the minimum amounts of residual gas trapped enabled the achievement of lean in-cylinder mixtures, with in-cylinder lambda values of up to 1.34. Conversely, fuel enrichment was necessary at higher engine speeds and mid-low loads to improve combustion stability. The in-cylinder lambda was found to greatly deviate from the exhaust lambda by an average factor of 1.8, so graphical and analytical approaches were provided for its estimation based on the Benson–Brandham scavenging model.

Acknowledgements The first and second authors would like to acknowledge the Brazilian council for scientific and technological development (CNPq–Brasil) for supporting their PhD studies at Brunel University London.

References

1. ExxonMobil (2017) Outlook for Energy 2017
2. International Council on Clean Transportation (ICCT) (2014) EU CO2 emission standards for passenger cars and light-commercial vehicles
3. Wei H, Shao A, Hua J, Zhou L, Feng D (2018) Effects of applying a Miller cycle with split injection on engine performance and knock resistance in a downsized gasoline engine. Fuel 214:98–107. https://doi.org/10.1016/j.fuel.2017.11.006
4. Zhao H (ed) (2010) Advanced direct injection combustion engine technologies and development. Woodhead Publishing Limited, Cambridge
5. Alvarez CEC, Couto GE, Roso VR, Thiriet AB, Valle RM (2018) A review of prechamber ignition systems as lean combustion technology for SI engines. Appl Therm Eng 128:107–120. https://doi.org/10.1016/j.applthermaleng.2017.08.118
6. Costa M, Sorge U, Merola S, Irimescu A, La Villetta M, Rocco V (2016) Split injection in a homogeneous stratified gasoline direct injection engine for high combustion efficiency and low pollutants emission. Energy 117:405–415. https://doi.org/10.1016/j.energy.2016.03.065
7. Smith J, Szekely G Jr, Solomon A, Parrish S (2011) A comparison of spray-guided stratified-charge combustion performance with outwardly-opening piezo and multi-hole solenoid injectors. SAE Int J Engines 4:1217–2011. https://doi.org/10.4271/2011-01-1217
8. Bhasker JP, Porpatham E (2017) Effects of compression ratio and hydrogen addition on lean combustion characteristics and emission formation in a Compressed Natural Gas fuelled spark

ignition engine. Fuel 208:260–270. https://doi.org/10.1016/j.fuel.2017.07.024
9. IEA International Energy Agency (2017) Global EV Outlook 2017. IEA. https://doi.org/10.1787/9789264278882-en
10. Fraidl GK, Beste F, Kapus PE, Korman M, Sifferlinger B, Benda V (2011) Challenges and solutions for range extenders—from concept considerations to practical experiences. https://doi.org/10.4271/2011-37-0019
11. Laget O, Ternel C, Thiriot J, Charmasson S, Tribotte P, Vidal F (2013) Preliminary design of a two-stroke uniflow diesel engine for passenger car. SAE Int J Engines 6:596–613. https://doi.org/10.4271/2013-01-1719
12. Benajes J, Novella R, De Lima D, Tribotté P, Quechon N, Obernesser P et al (2013) Analysis of the combustion process, pollutant emissions and efficiency of an innovative 2-stroke HSDI engine designed for automotive applications. Appl Therm Eng 58:181–193. https://doi.org/10.1016/j.applthermaleng.2013.03.050
13. Lu Y, Pei P, Liu Y (2014) An evaluation of a 2/4-stroke switchable secondary expansion internal combustion engine. Appl Therm Eng 73:323–332. https://doi.org/10.1016/j.applthermaleng.2014.07.075
14. Mattarelli E, Rinaldini CA, Cantore G, Agostinelli E (2014) Comparison between 2 and 4-stroke engines for a 30 kW range extender. SAE Int J Altern Powertrains 4:114–2014. https://doi.org/10.4271/2014-32-0114
15. Wu Y, Wang Y, Zhen X, Guan S, Wang J (2014) Three-dimensional CFD (computational fluid dynamics) analysis of scavenging process in a two-stroke free-piston engine. Energy 68:167–173. https://doi.org/10.1016/j.energy.2014.02.107
16. Jia B, Smallbone A, Zuo Z, Feng H, Roskilly AP (2016) Design and simulation of a two- or four-stroke free-piston engine generator for range extender applications. Energy Convers Manag 111:289–298. https://doi.org/10.1016/j.enconman.2015.12.063
17. Kock F, Haag J, Friedrich HE (2013) The free piston linear generator—development of an innovative, compact, highly efficient range-extender module. SAE Tech. Pap. https://doi.org/10.4271/2013-01-1727
18. Geng H, Wang Y, Zhen X, Liu Y, Li Z (2018) Study on adaptive behavior and mechanism of compression ratio (or piston motion profile) for combustion parameters in hydraulic free piston engine. Appl Energy 211:921–928. https://doi.org/10.1016/j.apenergy.2017.11.100
19. Yuan C, Ren H, Xu J (2017) Comparison of the gas exchange of a loop scavenged free-piston engine alternator and the conventional engine. Appl Therm Eng 127:638–649. https://doi.org/10.1016/j.applthermaleng.2017.08.059
20. Kee RJ, Blair GP, Douglas R (1990) Comparison of performance characteristics of loop and cross scavenged two-stroke engines. SAE Tech. Pap. https://doi.org/10.4271/901666
21. Hooper PR, Al-Shemmeri T, Goodwin MJ (2011) Advanced modern low-emission two-stroke cycle engines. Proc Inst Mech Eng Part D J Automob Eng 225:1531–1543. https://doi.org/10.1177/0954407011408649
22. Andwari AM, Aziz AA, Said MFM, Latiff ZA (2014) Experimental investigation of the influence of internal and external EGR on the combustion characteristics of a controlled auto-ignition two-stroke cycle engine. Appl Energy 134:1–10. https://doi.org/10.1016/j.apenergy.2014.08.006
23. Nakano M, Sato K, Ukawa H (1990) A two-stroke cycle gasoline engine with poppet valves on the cylinder head. SAE Tech. Pap., vol 99, pp 1972–84. https://doi.org/10.4271/901664
24. Hundleby GE (1990) Development of a poppet-valved two-stroke engine—the flagship concept. SAE Tech. Pap. https://doi.org/10.4271/900802
25. Nomura K, Nakamura N (1993) Development of a new two-stroke engine with poppet-valves: Toyota S-2 engine. In: Duret P (ed) A new Gener. two-stroke engines futur., Technip, Paris, pp 53–62
26. Carlucci AP, Ficarella A, Laforgia D, Renna A (2015) Supercharging system behavior for high altitude operation of an aircraft 2-stroke diesel engine. Energy Convers Manag 101:470–480. https://doi.org/10.1016/j.enconman.2015.06.009
27. Benajes J, Molina S, Novella R, De Lima D (2014) Implementation of the partially premixed combustion concept in a 2-stroke HSDI diesel engine fueled with gasoline. Appl Energy 122:94–111. https://doi.org/10.1016/j.apenergy.2014.02.013
28. Miles SR, Ghandhi JB (2016) Investigation of reactivity-controlled compression ignition combustion in a two-stroke engine. Proc Inst Mech Eng Part D J Automob Eng 230:1835–1848. https://doi.org/10.1177/0954407015624554
29. Sher E (1990) Scavenging the two-stroke engine. Prog Energy Combust Sci 16:95–124. https://doi.org/10.1016/0360-1285(90)90045-5
30. Merker GP, Gerstle M (1997) Evaluation on two stroke engines scavenging models. https://doi.org/10.4271/970358
31. Benson RS, Brandham PT, Brandham PJ, Benson RS (1969) A method for obtaining a quantitative assessment of the influence of charging efficiency on two-stroke engine performance. Int J Mech Sci 11:303–312. https://doi.org/10.1016/0020-7403(69)90048-4
32. Čudina M (2004) Model testing the two-phase scavenging system in a two-stroke petrol engine. Proc Inst Mech Eng Part D J Automob Eng 218:1307–1316. https://doi.org/10.1243/0954407042579978
33. Li ZH, He BQ, Zhao H (2014) Application of a hybrid breakup model for the spray simulation of a multi-hole injector used for a DISI gasoline engine. Appl Therm Eng 65:282–292. https://doi.org/10.1016/j.applthermaleng.2013.12.063
34. Heywood JB (1988) Internal combustion engine fundamentals. McGraw-Hill, New York
35. Eng JA (2002) Characterization of pressure waves in HCCI combustion. SAE Tech. Pap. https://doi.org/10.4271/2002-01-2859
36. Xie H, Li L, Chen T, Yu W, Wang X, Zhao H (2013) Study on spark assisted compression ignition (SACI) combustion with positive valve overlap at medium–high load. Appl Energy 101:622–633. https://doi.org/10.1016/j.apenergy.2012.07.015
37. Dalla Nora M, Lanzanova TDM, Zhao H (2018) Four-valve supercharged two-stroke DI engine fuelled with gasoline and ethanol. Fuel 227c:401–411. https://doi.org/10.1016/j.fuel.2018.04.078
38. Dalla Nora M, Zhao H (2015) High load performance and combustion analysis of a four-valve direct injection gasoline engine running in the two-stroke cycle. Appl Energy 159:117–131. https://doi.org/10.1016/j.apenergy.2015.08.122
39. Silvis WM (1997) An algorithm for calculating the air/fuel ratio from exhaust emissions. SAE Tech. Pap. https://doi.org/10.4271/970514
40. Taylor CF (1985) The internal combustion engine in theory and practice, vol II, 2nd edn. MIT Press, Cambridge
41. Olsen DB, Hutcherson GC, Willson BD, Mitchell CE (2002) Development of the tracer gas method for large bore natural gas engines—part I: method validation. J Eng Gas Turbines Power 124:678. https://doi.org/10.1115/1.1454116
42. Olsen DB, Hutcherson GC, Willson BD, Mitchell CE (2002) Development of the tracer gas method for large bore natural gas engines—part II: measurement of scavenging parameters. J Eng Gas Turbines Power 124:686. https://doi.org/10.1115/1.1454117
43. Blair GP (1996) Design and simulation of two-stroke engines. Society of Automotive Engineers, Warrendale
44. Douglas R (1990) AFR and emissions calculations for two-stroke cycle engines. SAE Tech. Pap. https://doi.org/10.4271/901599
45. Mattarelli E, Cantore G, Rinaldini CA, Savioli T (2017) Combustion system development of an opposed piston 2-stroke

diesel engine. Energy Procedia 126:1003–1010. https://doi.org/10.1016/j.egypro.2017.08.268
46. Naik S, Redon F, Regner G, Koszewnik J (2015) Opposed-piston 2-stroke multi-cylinder engine dynamometer demonstration. SAE Tech. Pap., 2015. https://doi.org/10.4271/2015-26-0038
47. Kim N, Cho S, Choi H, Song HH, Min K (2014) The efficiency and emission characteristics of dual fuel combustion using gasoline direct injection and ethanol port injection in an SI engine. SAE Tech. Pap., 2014. https://doi.org/10.4271/2014-01-1208
48. Stone R (2012) Introduction to internal combustion engines, 4th edn. Palgrave Macmillan, Basingstoke
49. Martin S, Beidl C, Mueller R (2014) Responsiveness of a 30 Bar BMEP 3-cylinder engine: opportunities and limits of turbocharged downsizing. SAE Tech. Pap., 2014. https://doi.org/10.4271/2014-01-1646
50. Nora MD, Lanzanova TDM, Zhao H (2016) Effects of valve timing, valve lift and exhaust backpressure on performance and gas exchanging of a two-stroke GDI engine with overhead valves. Energy Convers Manag. https://doi.org/10.1016/j.enconman.2016.05.059
51. Li Z, He B, Zhao H (2014) The influence of intake port and pent-roof structures on reversed tumble generation of a poppet-valved two-stroke gasoline engine. SAE Tech Pap 2014. https://doi.org/10.4271/2014-01-1130
52. Huh KY, Kim KK, Choi CR, Park SC, Moon S, Lee KY (1993) Scavenging flow simulation of a four-poppet-valved two-stroke engine. SAE. https://doi.org/10.4271/930500